Advances in Science and Technology Research Journal

Advances in Science and Technology Research Journal, 2026, 20(3), 559–573
https://doi.org/10.12913/22998624/214338
ISSN 2299-8624, License CC-BY 4.0

Received: 2025.11.04
Accepted: 2025.12.17
Published: 2026.02.01

Analysis of the stress triaxiality impact on the fatigue strength of a structural component with machine learning tools

Mariusz Janusz-Bielecki[1], Jaroslaw Galkiewicz[1*]

[1] Faculty of Mechatronics and Mechanical Engineering, Kielce University of Technology, Aleja Tysiaclecia Panstwa Polskiego 7, 25-314 Kielce, Poland
* Corresponding author's e-mail: jgalka@tu.kielce.pl

ABSTRACT

This article uses machine learning tools to analyze mechanical field parameters for their impact on the fatigue strength of a structural component. After selecting the geometry, characteristic dimensions were varied to obtain different values of the theoretical notch shape factor. These values were determined using formulas. Finite element simulations were performed for each set of changed dimensions to obtain mechanical field parameters. After establishing a database of mechanical field parameters, their impact on the high-cycle fatigue strength of structural components was determined. It turned out that an important parameter from a fatigue strength point of view is stress triaxiality. The results indicate that for the selected geometry the model explains as much as 97.84% of the variance of the target variable (shape factor), which is a very good result and encourages further analyses for other geometries. The described machine learning application has not been used in the way presented so far, and a positive result will allow replacing the geometry-dependent formulas used to determine the shape factor with a new unified approach based on the stress triaxiality.

Keywords: high-cycle fatigue, fatigue strength, stress triaxiality, machine learning, finite element method, actual safety factor.

INTRODUCTION

Over the years of operation of various engineering structures, a phenomenon of their destruction under stresses with values significantly lower than the strength limit of the material from which they were manufactured has been observed. Results of laboratory tests or analyses using computational methods confirmed the occurrence of this phenomenon in structural components of building objects, industrial machines, means of transportation, and pressure equipment. It was discovered that such failures arise as a result of a cracking process occurring without the presence of plastic deformations [1] or with their participation, but limited to small areas [2]. The described damage was associated with cyclic loads. Their consequence was a significant reduction in the service life of structures.The pursuit of determining the life of structural elements subjected to loads characterized by variability in magnitude and/or direction of applied forces has led to the development of a new research area related to the problem of material fatigue. This discipline takes into account, among other things, the influence of cyclic loads on the service life, which is defined as fatigue life.

In order to determine fatigue life, computational analyses of structural components are carried out using methodologies based on theories such as continuum mechanics, plasticity theory, and fracture mechanics. These methodologies are developed based on theoretical research, results of laboratory experiments, and operational experience of various technical objects, covering areas such as high-cycle fatigue strength, low-cycle fatigue strength, and crack propagation kinetics. Issues related to fatigue calculations have been presented in numerous dedicated publications, including book monographs e.g. [3-5]. Additionally, they also appear in works devoted to structural

mechanics, materials strength science, or the design of machines, pressure vessels, construction products, and other engineering structures [1, 6].

Fatigue-type loads are a frequent cause of failure in numerous structures. This phenomenon is the subject of research, among other reasons, due to its impact on the safety of operated structures, equipment, and technical installations. Fatigue characteristics of materials are commonly expressed through fatigue life and fatigue limit determined based on a graph showing stress amplitude as a function of the number of cycles leading to failure. This is the most often presented in the form of a Wöhler curve (S-N). Structural damage as a result of fatigue phenomena is caused, among other things, by degradation of the material from which they are made. Fatigue failure process of slow growth of cracks is initiated in existing microstructural defects. This process can be accelerated by local stress concentrations [7] or chemically assisted stress corrosion [8]. In materials with elastic-plastic properties, the condition for the occurrence of this type of damage is the appearance, growth, and coalescence of microcracks and voids occurring in them [9]. Fatigue damage to structural elements is influenced not only by forces and force moments, surface condition, or detail dimensions, but also by external operating conditions, such as the medium surrounding the structure, temperature, amplitude of interactions, and their character [10–12].

Measurements of fatigue crack growth kinetics are commonly performed on specimens containing notches. Fatigue tests are characterized by long duration, and their results are influenced by many factors, often independent of the adopted research methodology. This means that fatigue research requires the involvement of experienced specialists who should use specialized equipment. The preparation and implementation of fatigue research takes significantly longer time than quasi-static tests, such as tensile strength tests.

For elements subjected to fatigue, the actual (real) safety factor is determined, whose value depends on many factors. The most important of these are: geometry, presence of stress concentrators, element dimensions, surface layer condition, environmental characteristics of the detail such as temperature or corrosion effects, as well as several others. In this work, only selected factors from those mentioned will be discussed in detail.

Notches, also called stress concentrators, constitute various types of material dis-continuities occurring in cross-sections of the analyzed structural element, which cause local stress increase in their immediate vicinity. Stress concentration means local increase in stress values appearing in the vicinity of holes, constrictions, cracks, and sharp shape discontinuities of the cross-section [13].

The mechanism of action of stress concentrators consists in disrupting the natural flow of stresses in the material structure, which results in local increase of their values exceeding the level of nominal stresses. Detailed analyses indicate that in areas of stress concentration, stresses can reach magnitudes several times greater than those calculated for the zone outside this area. In places where stress concentrations occur, the material structure becomes weakened and susceptible to the formation of cracks and fractures leading to local damage, particularly under dynamic or variable loading conditions [14].

Stress concentrators have a fundamental impact on the formation of non-uniform stress distribution within the cross-section in which they are located [15]. The occurrence of a result of which the maximum actual stress at the notch root significantly exceeds the nominal stress of the element, and the fatigue failure process most often begins precisely at this location. A series of parameters are used for their characterization. The first of these, which should be discussed, is the theoretical stress concentration factor for normal stresses (tension, bending), defined as follows:

$$\alpha_k = \frac{\sigma_{max}}{\sigma_{nom}} \tag{1}$$

where: σ_{max} is the maximum stress caused by the notch, and σ_{nom} is the nominal stress.

This coefficient is sometimes referred to as the notch shape factor. Another one is the effective stress concentration factor or notch action factor defined as:

$$\beta_k = \frac{Z_{gl}}{Z_k} \tag{2}$$

where: Z_{gl} is the fatigue limit of a smooth specimen, and Z_k is the fatigue limit of a notched specimen.

Both coefficients, i.e., the notch shape factor and the notch action factor, are related by the material sensitivity factor to notch action η_k (3), introduced several decades ago [16]:

$$\eta_k = \frac{\beta_k - 1}{\alpha_k - 1} \tag{3}$$

hence:

$$\beta_k = 1 + \eta_k(\alpha_k - 1) \tag{4}$$

The coefficient η_k is most often determined from graphs depending on tensile strength R_m and notch radius ρ [17]. Fatigue strength usually decreases with increasing element dimensions. However, there is a lack of complete theoretical explanation of this phenomenon. In practice, metallurgical and technological factors have a strong influence, regardless of the element's shape or size. The relationship between object size and its fatigue life is often described in a probabilistic way, referring to the weakest link theory. It is defined using the object size coefficient ε:

$$\varepsilon = \frac{Z_d}{Z} \tag{5}$$

where: Z_d is the strength of a specimen with any diameter d, and Z is the strength of a specimen made from the same material with a diameter of 7 to 10 mm [18].

Every type and method of surface treatment affects the fatigue life of the material. This results both, from the surface shape and from a set of complex physical processes occurring in the surface layer during treatment, e.g., plastic treatment or machining. Treatment residues usually form regular, repeating micro-notches. The action of these notches is additionally reinforced by the occurrence of residual stresses resulting mainly from plastic deformation of the layer, which can lead to its local hardening or weakening. The surface condition coefficient β_p is defined as:

$$\beta_p = \frac{Z_0}{Z_p} \tag{6}$$

where: Z_0 is the strength of a polished specimen, and Z_p is the strength of a specimen made from the same material after various treatments [19].

In 1904, a Polish scientist from Lwów University of Technology, Tytus Huber, first proposed the hypothesis that material strength is a function of on the energy stored in the deformed material. This energy is proportional to the second invariant of the stress deviator, according to the formula:

$$E_o \sim J_2 \tag{7}$$

which, in turn, can be represented using equivalent stress, as follows:

$$\sigma_{eHMH} = \sqrt{\frac{1}{2}[(\sigma_{11} - \sigma_{22})^2 + (\sigma_{22} - \sigma_{33})^2 + (\sigma_{33} - \sigma_{11})^2] + 3(\tau_{12}^2 + \tau_{23}^2 + \tau_{31}^2)} \tag{8}$$

where: σ and τ are stress tensor components. In the principal stress space, the equivalent stress has the following form:

$$\sigma_{eHMH} = \sqrt{\frac{1}{2}[(\sigma_1 - \sigma_2)^2 + (\sigma_2 - \sigma_3)^2 + (\sigma_3 - \sigma_1)^2]} \tag{9}$$

Using contemporary terminology, we would say that material failure occurs when the reduced stress reaches a critical value. The parameter defining the stress triaxiality appeared in the mid-20th century. Two scientists, Davies and Connelly, published a work in 1959 in which they used this parameter [20]. The authors defined the stress triaxiality as the ratio of the first invariant of the stress tensor to the reduced stress as follows:

$$\eta_{DC} = \frac{\sigma_m}{\sigma_e} = \frac{I_1}{\sqrt{3J_2}} \tag{10}$$

where: σ_m is the hydrostatic stress and is σ_e the equivalent stress according to the Huber-Mises-Hencky hypothesis (HMH).

The motivation for introducing the stress triaxiality parameter was their conviction, supported by experimental results, that the hydrostatic stress has a strong influence on the loss of plasticity in metals. At the beginning of the 21st century, the stress triaxiality was used in the description of metal plasticity [21–23]. Many articles have evaluated critical stress using stress triaxiality. It turned out that this quantity could be used to predict fatigue crack initiation [15] and fatigue crack growth [24], however, the number of observations is not convincing.

In recent years, the use of machine learning to discover relationships that are difficult to detect traditionally has become increasingly popular. While these techniques require a significant amount of data and computational power, the results are significant. In [25], a neural network was trained to determine the peak shape factor values with very high accuracy in a complex welded joint subjected to complex loads, and in [26], again using a neural network, formulas for the shape factor for a tubular T-joint were obtained. Besides solving computational problems, machine learning techniques can also be used in more practical ways, for example, for crack localization [27].

In the presented work, the application of the scalar field distribution of stress state triaxiality

in the analysis of fatigue strength of a selected structural element related to real safety factor was presented. Analysis of stress triaxiality can contribute to simplifying and shortening laboratory tests used in everyday engineering practice. For this purpose, modeling and numerical calculations were used, as well as machine learning for inferring the fatigue strength of selected structural components. Within the framework of achieving this goal, it was decided to:

- select a working environment equipped with appropriate computational tools,
- select a structural element subjected to further analysis and evaluation,
- determine the variability of geometric parameters of the structural element and the variability of the theoretical stress concentration factor α,
- implement modeling of the geometry of the selected structural element,
- select boundary conditions for the element, including displacement constraints and force loads,
- perform numerical calculations of the structural element using the finite element method,
- subject the obtained calculation results to preliminary analysis in order to prepare training and testing datasets for machine learning algorithms,
- implement the machine learning process using the linear regression method,
- perform verification of the obtained data,
- perform validation of the obtained results in relation to the actual (real) safety factor under fatigue conditions of the selected structural element.

MATERIALS AND METHODS

Machine learning is a data processing technique that automates the creation of analytical models. It belongs to the field of artificial intelligence and is based on the assumption that systems can learn independently from data, recognize patterns, and make decisions with minimal human involvement. The most important feature of machine learning is the abandonment of manual programming of specific tasks. Instead, algorithms construct a mathematical model based on example data, called the training set, to predict outcomes or make decisions. One of the frequently used tasks in machine learning is regression.

Regression

The regression task involves predicting a continuous variable by learning a function or algorithm that most faithfully reproduces the training data. After the training phase, the model creates its own representation space. New observations are projected into it, enabling their analysis and forecasting based on patterns acquired during training. Regression serves to predict numerical values of real-world processes based on previous data. It enables detection of dependencies between variables, which is essential in making data-driven decisions.

In machine learning, various types of regression are distinguished, adapted to the type of data and degree of problem complexity:

- linear regression assumes a simple, linear relationship between variables. It is fast and easy to interpret;
- polynomial regression introduces polynomials into the fitting function, allowing modeling of non-linearity. However, it requires caution to avoid over-fitting;
- isotonic regression enforces monotonic increase or decrease in the predicted value. It is used in fields such as biology, economics, medicine, and psychology;
- logistic regression serves classification purposes. It predicts the probability of belonging to a given class. It is common in medicine, marketing, and social research.

Through the application of various algorithms, regression forms the foundation of data analysis and machine learning. It allows not only forecasting but also better understanding of complex relationships in data and supports accurate decisions in various fields of science, business, and daily life.

Evaluation metrics

In assessing the effectiveness of machine learning models for regression tasks, four metrics are commonly used. Each measures prediction errors in a different way and provides slightly different perspectives on the model's fit quality to the data. These metrics include:

- mean absolute error (MAE);
- mean squared error (MSE);
- root mean squared error (RMSE);
- coefficient of determination R^2, which, in the case of linear regression, equals the square of the Pearson correlation coefficient.

Numerical calculations

The research on the influence of the stress-triaxiality field distribution was carried out in several stages, with the results of each stage serving as input for the next. Within this framework, the tasks were performed:

- a structural component was selected and the range of its geometric variations was defined;
- for each specimen, depending on its shape and loading conditions, the theoretical notch-shape factor α was calculated using Python programs (Spyder environment), and the components were modeled in the Salome platform (Geometry module) with parametric modeling;
- a Python (Spyder) tool was created to generate the mesh in Salome's Smesh module. Finite-element analyses were then performed and the data were prepared for post-processing in Code_Aster;
- the results were verified in the ParaView post-processor
- a Python (Spyder) application was developed to organize and prepare the post-processing data for machine-learning purposes;
- a supervised linear-regression model for machine learning was implemented in Python (Spyder);
- final verification and validation of the obtained results were carried out in the Spyder environment.

Based on the literature [2, 13, 28], the selected structural element is a flat specimen with a central hole, for which the values of notch shape factors are known. This type of element is commonly used in machines, pressure vessels, and construction products.

The decision to use a flat specimen with a hole resulted from the need to reproduce real operating conditions and analyze the influence of various notch shape factors (stress concentrators) on fatigue life.

The geometry of the specimen with a hole enables simple observation of initiation and development of fatigue cracks around the hole. Research proves that the fatigue life of such specimens is approximately 3–4 times lower than specimens without a hole, which highlights the significant role of stress concentrators in the fatigue resistance of the material [2]. Easy manufacturing and testing of this type of specimen allows for increasing the number of tests while maintaining repeatability of results.

The flat element (flat specimen) was shown in Figure 1. A constant thickness p_t = 10 mm was adopted for the tests. The circular hole was positioned centrally. Its radius h_r (circular hole diameter) varied from 2 mm to 23 mm with a step equal to 1 mm. The width of the elements p_w used for testing ranged from 50 mm to 165 mm with a step equal to 5 mm.

Based on the selected specimen, the boundary conditions, the supports and applied loads were defined. The flat element with a centrally located circular hole was subjected exclusively to an axial tensile force F_x. The global coordinate system was placed on one of the specimen's faces, with its origin at the midpoint of the thickness along the z-axis and at half the width along the Y-axis. Each coordinate axis was parallel to one of the element's edges. A view of the global coordinate system and the boundary conditions for this element is shown in Figure 2.

Boundary conditions in the form of kinematic constraints were imposed according to the scheme given in Table 1. The load in the form of a force was applied along the axis and on the surface opposite the plane YZ at distance of 100 mm.

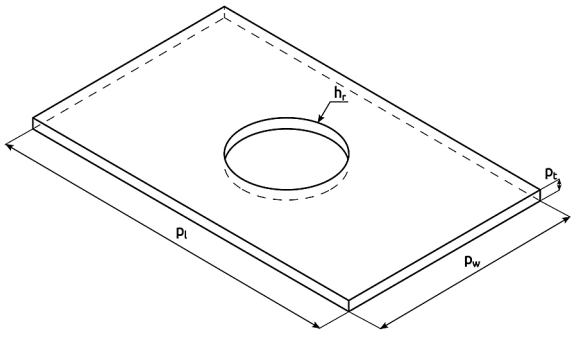

Figure 1. Flat element with a circular hole. Description in the text

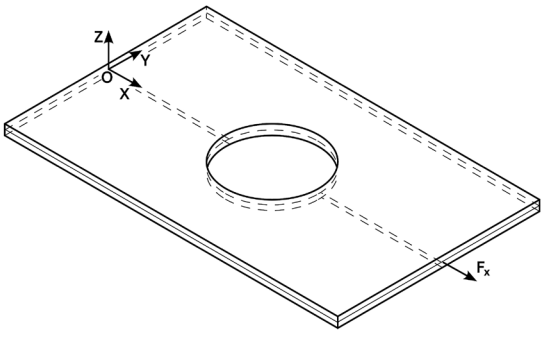

Figure 2. Flat element with a circular hole. Boundary conditions

Table 1. Boundary conditions of flat specimen with circular hole

Location	Condition	Value
XY plane constraints	coordinates z	0 mm
XZ plane constraints	coordinates y	0 mm
YZ plane constraints	coordinates x	0 mm
Force perpendicular to the surface opposite to YZ, at a distance of 100 mm, according to Figure 2.	Fx	1000 N

According to [28], the relationship for the theoretical notch shape factor in the case of an axial tensile force applied along the element's longitudinal axis is given by Equation 11. The notation in the formula corresponds to Figure 1 and Table 2.

$$\alpha = 3.00 - 3.13\left(\frac{2h_r}{p_w}\right) + \\ + 3.66\left(\frac{2h_r}{p_w}\right)^2 - 1.53\left(\frac{2h_r}{p_w}\right)^3 \qquad (11)$$

A surface plot of the notch shape factor for the flat specimen with a circular hole is shown in the Figure 3, as a function of the specimen width and the hole radius.

Table 2 presents all relevant geometric parameters of the flat element with a centrally located circular hole. Additionally, it indicates the quantities of specimens in relation to significant parameters, namely width and hole radius, as well as the range of variability of the theoretical notch shape factor α.

After selecting various element variants, a comprehensive Python application was developed, leveraging the advanced parametric solid-modeling capabilities of Salome platform's Geometry module. By implementing this application, it was possible to automatically generate 528 distinct specimens of the structural element under study.

Numerical calculations were carried out using a Python application run in the Spyder scientific environment. Mesh generation with refinement was performed in Salome. The Smesh module was used. After meshing, the application conducted FEM (finite element method) analyses in Code_Aster and prepared the data for the post-processor.

In Figures 4–7 the specimens with their meshes and the field of stress triaxiality are shown. On these figures, the triaxiality scale is labeled as reslin_SIEQ_NOEU. In Code_Aster, this defines reduced stress fields averaged over all elements adjacent to a given mesh node. They form continuous, smoothed stress fields at the nodes–facilitating visualization of the overall stress distribution at the

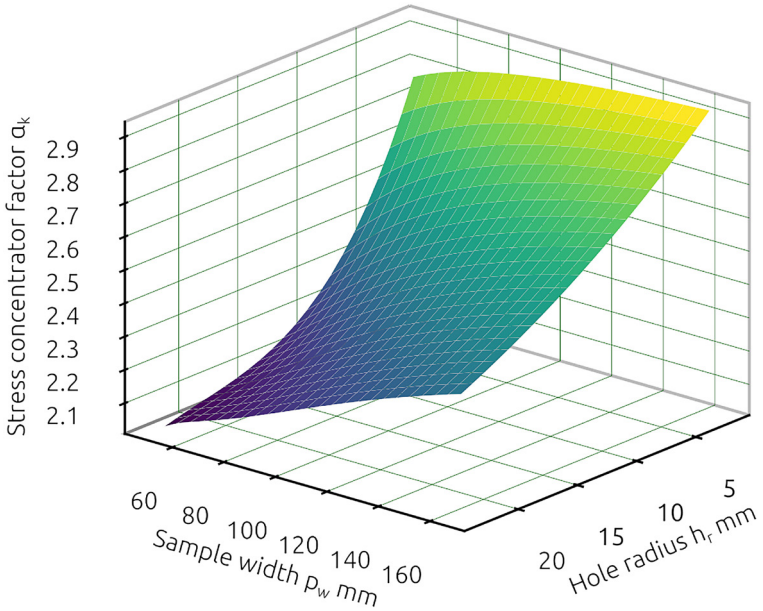

Figure 3. Theoretical notch shape factor α variety

Table 2. Flat element with circular hole parameters

Parameter	Symbol	Value	Variety
Thickness	p_t	10 mm	constant
Length	p_l	100 mm	constant
Width	p_w	50 mm – 165 mm interval 5 mm	22 samples
Circular hole	h_r	2 mm – 23 mm interval 1 mm	24 samples
Theoretical notch shape factor, tension	α	2.02 at h_r=23 and p_w=50 2.37 at h_r=23 and p_w=165 2.77 at h_r=2 and p_w=50 2.92 at h_r=2 and p_w=165	528 samples

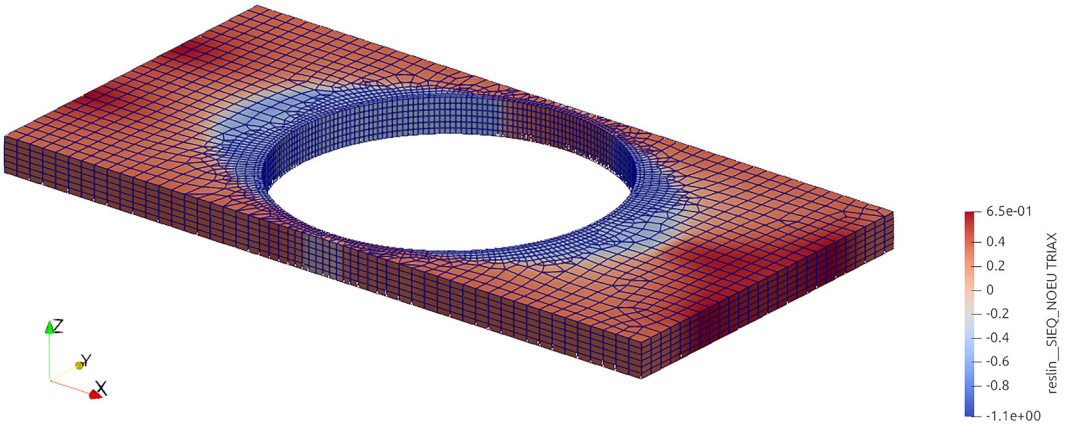

Figure 4. FEM analysis results, 23_50

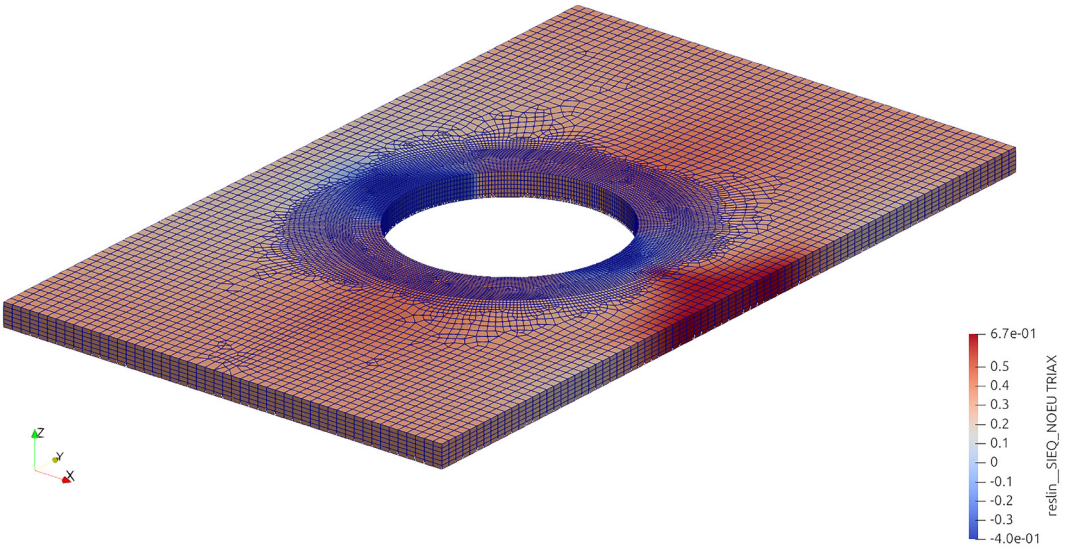

Figure 5. FEM analysis results, 23_165

expense of partial loss of extreme-value accuracy. The term TRIAX denotes stress-state triaxiality.

All finite-element computations employed the linear static analysis operator MECA_STATIQUE. MECA_STATIQUE is Code_Aster's main operator for performing linear static analyses of solid-mechanics problems. It solves the equilibrium equations under static loads, optionally accounting for temperature-dependent material properties. In this work, temperature effects on the stress field were

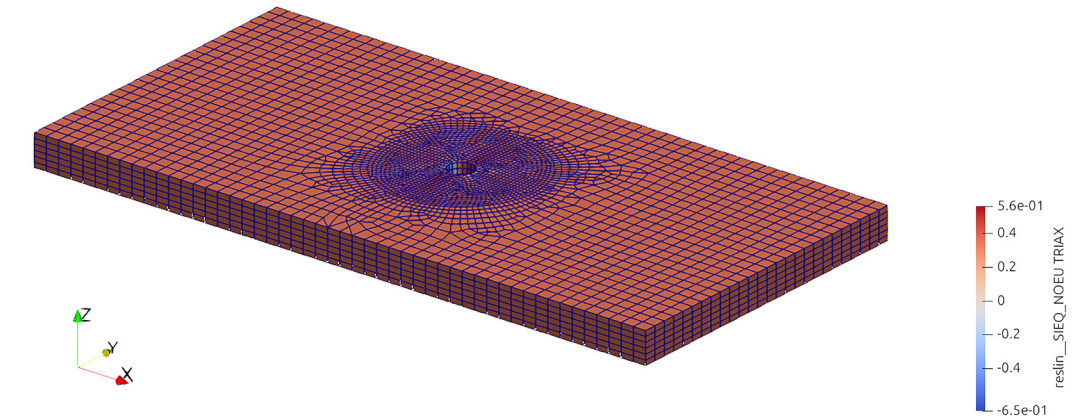

Figure 6. FEM analysis results, 2_50

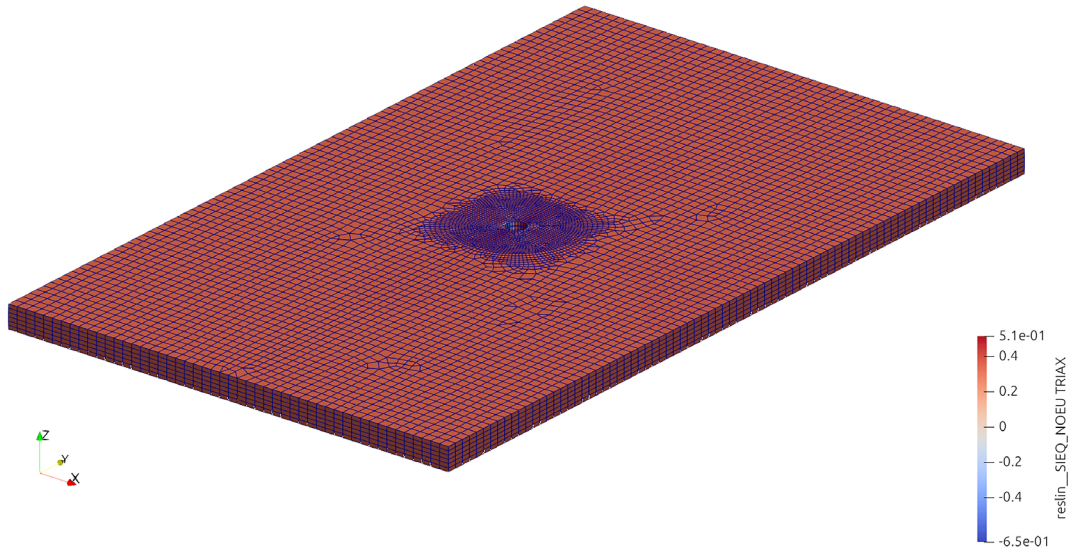

Figure 7. FEM analysis results, 2_165

not considered. MECA_STATIQUE computes displacements, stresses, and strains in structures under the assumptions of small deformations and linear material elasticity. This operator allows the application of multiple boundary conditions and various load types, such as forces, pressures, and prescribed displacements in a single calculation run. Its output is an object containing the nodal displacement field for the zero step. MECA_STATIQUE is optimized for linear analyses, offering rapid convergence for small-deformation problems. It assumes linear material behavior and omits iterative load steps. Stress and strain fields require the subsequent operator CALC_CHAMP, which transforms the primary FEM results (i.e., displacements) into useful quantities such as stresses (including reduced stresses), strains, and reactions. CALC_CHAMP is essential in virtually every structural analysis where assessment of element strength or stress state is needed.

RESULTS

In this subsection, the results of the analysis of flat structural elements with a centrally located circular hole, one case are presented. A three-dimensional, polyhedral mesh was used. The dominant type chosen was eight-node hexahedra. These were complemented by six-node triangular-prism elements. In regions where stress concentrations were expected, the mesh was refined by halving the element size relative to the global minimum size. The graphical results of the analyses include the four extreme stress triaxiality distributions

corresponding to the notch shape factor α. These are shown in the same view and on the same scale for easier comparison. The Table 3 provides information on the specimen parameters, the notch shape factor α, and the figures of the elements. A Python application was prepared for the numerical calculations, which generated text files for each element as output. These files contained the principal values of spatial stress tensor. Additionally, HMH equivalent stress values (Equation 8) were computed, enabling the determination of stress-state triaxiality for all finite-element sample elements. The resulting files formed the basis for subsequent work. After the numerical calculations, a text file was obtained containing, for all specimens and their finite elements:

- the principal stress values of the stress tensor.
- the reduced stress values according to the HMH hypothesis,
- the stress-state triaxiality values.

This file was used by a Python application to generate histograms of the stress-state triaxiality for each specimen. In the remainder of this subsection, for those specimens whose notch shape factors α assumed extreme values, the aforementioned triaxiality histograms are plotted. These are hereafter also referred to simply as triaxiality histograms. The histograms of the stress-state triaxiality distributions are presented for the structural elements with a centrally located circular hole in Figures 8–11. Table 4 presents all statistical measures for the specimens with a hole for which the notch shape factor α assumed extreme values. The statistical analysis shown includes a comprehensive set of descriptive parameters, enabling a detailed description of the distribution of stress-state triaxiality in the investigated structural element.

During numerical calculation analysis, the statistical measures of stress state triaxiality for the specimen were obtained. These measures include the mean, mode, median, standard deviation, skewness, and kurtosis. This enabled the generation of training and validation datasets for machine learning.

Histograms are a fundamental tool for extracting and presenting data distribution in

Table 3. Parameters of the flat element with a circular hole

File	Hole radius hr	Specimen width pw	Notch shape factor α	Figure
23_50	23	50	2.02	4
23_165	23	165	2.37	5
2_50	2	50	2.77	6
2_165	2	165	2.92	7

Table 4. Statistical measures of triaxiality for circular hole specimens

Sample	Hole radius h_r	Width p_w	Notch factor α	Mean
23_50	23	50	2.026	0.010
Mode	Median	Deviation	Skewness	Kurtosis
0.308	0.122	0.355	-0.028	-1.656
Sample	Hole radius h_r	Width p_w	Notch factor α	Mean
23_165	23	165	2.378	0.240
Mode	Median	Deviation	Skewness	Kurtosis
0.334	0.309	0.205	-1.585	2.048
Sample	Hole radius h_r	Width p_w	Notch factor α	Mean
2_50	2	50	2.772	0.327
Mode	Median	Deviation	Skewness	Kurtosis
0.349	0.333	0.047	-9.929	149.530
Sample	Hole radius h_r	Width p_w	Notch factor α	Mean
2_165	2	165	2.926	0.330
Mode	Median	Deviation	Skewness	Kurtosis
0.333	0.333	0.036	-14.537	302.586

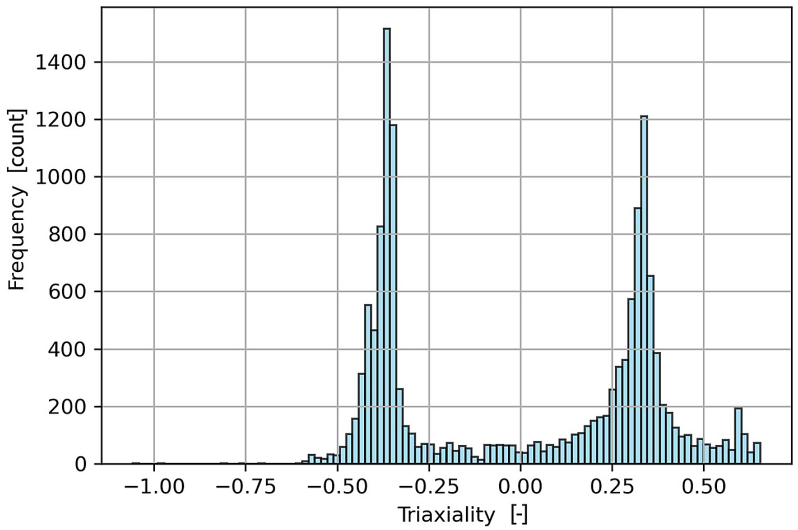

Figure 8. Flat specimen triaxiality histogram, 23_50

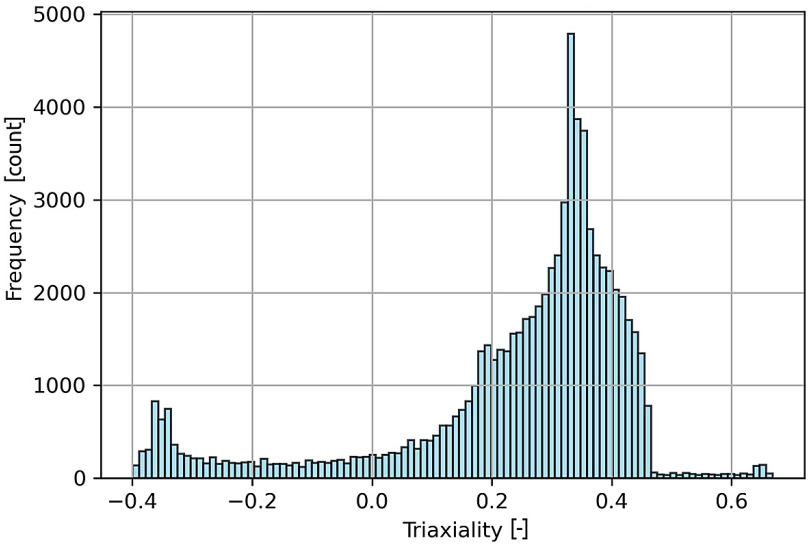

Figure 9. Flat specimen triaxiality histogram, 23_165

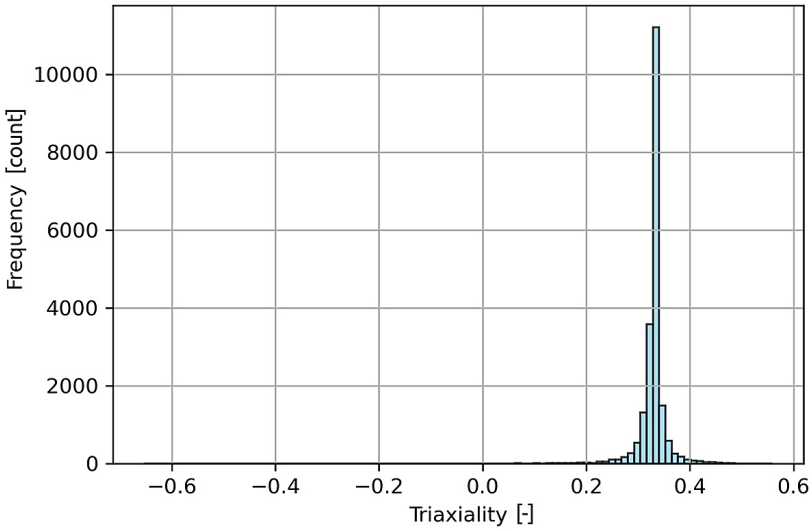

Figure 10. Flat specimen triaxiality histogram, 2_50

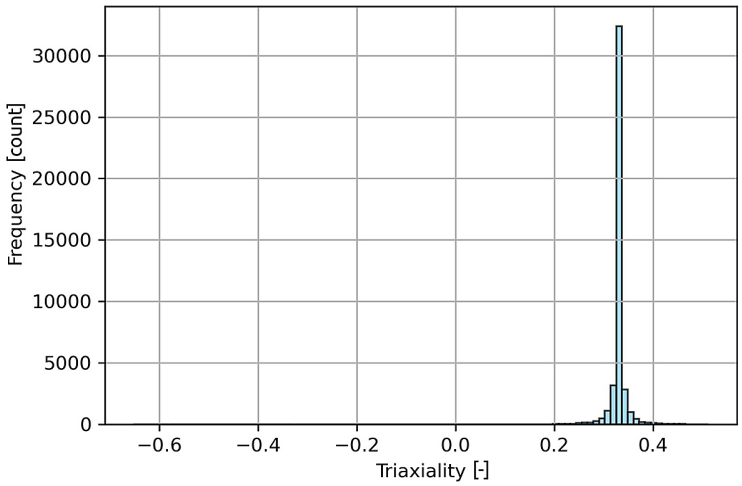

Figure 11. Flat specimen triaxiality histogram, 2_165

statistical analysis, enabling graphical visualization of the frequency of occurrence of individual values in the analyzed dataset. In the case of stress-state triaxiality studies, histograms enable the detection of characteristic stress distribution patterns in different parts of the specimen and estimation of how notch shape affects local stress states.

The obtained histograms of stress triaxiality distribution show clear variability related to the notch shape factor value, which demonstrates the complex nature of the relationship between notch geometry and local stress state. This diversity of distributions reflects different stress concentration mechanisms characteristic of various geometric configurations, with each notch form determining its own specific distribution of stress triaxiality values. Linear regression was selected for the machine learning task. The regression task involves predicting the value of a continuous variable based on a machine learning algorithm. A regression model can determine how the predicted quantity changes depending on the selected features describing the data. Regression is particularly useful in the analysis and evaluation of continuous variables.

This basic type of task was chosen because it enables obtaining key information about the structure of training data already at an early stage of the project. Through simple regression experiments, it can be quickly verified whether there are dependencies between input features and the target that can be captured by linear or non-linear models.

Training datasets were created by dividing the data of the specimen. For the regression task, a 3:1 split was applied, meaning 0.75 of the dataset constituted the training set and 0.25 of the dataset the test set. Table 5 presents the adopted divisions in relation to each of the two tasks.

At the beginning of the machine learning process, the capability of plotting heatmaps of datasets containing statistical measures of stress-state triaxiality was utilized. These were:

- mean (mean triaxiality),
- mode (triaxiality mode),
- median (triaxiality median),
- standard deviation (triaxiality standard deviation),
- skewness (triaxiality skew),
- kurtosis (triaxiality kurtosis),
- normalized skewness (triaxiality skew scaler),
- normalized kurtosis (triaxiality kurtosis scaler).

Heatmaps are available in the Seaborn library. They constitute one of the most powerful visualization tools in machine learning. They serve to understand relationships between features and labels. The heatmap function in the Seaborn library provides an intuitive way to visualize complex data matrices through color-coded representation. Correlation values in heatmaps range -1 to 1:

- a value of 1 indicates perfect positive correlation,

Table 5. Data set divisions according to task

Task	Dataset quantity	Training dataset	Testing dataset
Regression	528	396 (0.75 × 528)	132 (0.25 × 528)

- a value of 0 indicates no linear correlation between variables,
- a value of -1 indicates perfect negative correlation.

The presented heatmap visualizes Pearson correlation coefficients between multiple features in the dataset. This enables analysis of input data for machine learning. Figure 12 shows the heatmap containing all parameters of the flat specimen with a circular hole.

DISCUSSION

The correlation coefficients of the notch shape factor α with other parameters range from weak 0.32 to very strong 0.95. Hole radius. The relationship between hole radius and the notch shape factor α shows a strong inverse correlation of 0.85, which explains 72.2% of the variability. This seemingly counter-intuitive relationship suggests that larger holes may cause lower stress concentration factors, which can be explained by geometric scaling effects and the ratio of hole diameter to plate width.

Plate width. Plate width shows a moderate positive correlation 0.48 with stress concentration, explaining 23% of the variability. This relationship aligns with FEM analysis results, which show that narrower plates experience higher stress concentrations due to edge effects and limited capacity for load and stress redistribution.

Mean triaxiality. The mean triaxiality parameter shows the second-largest correlation of 0.91.

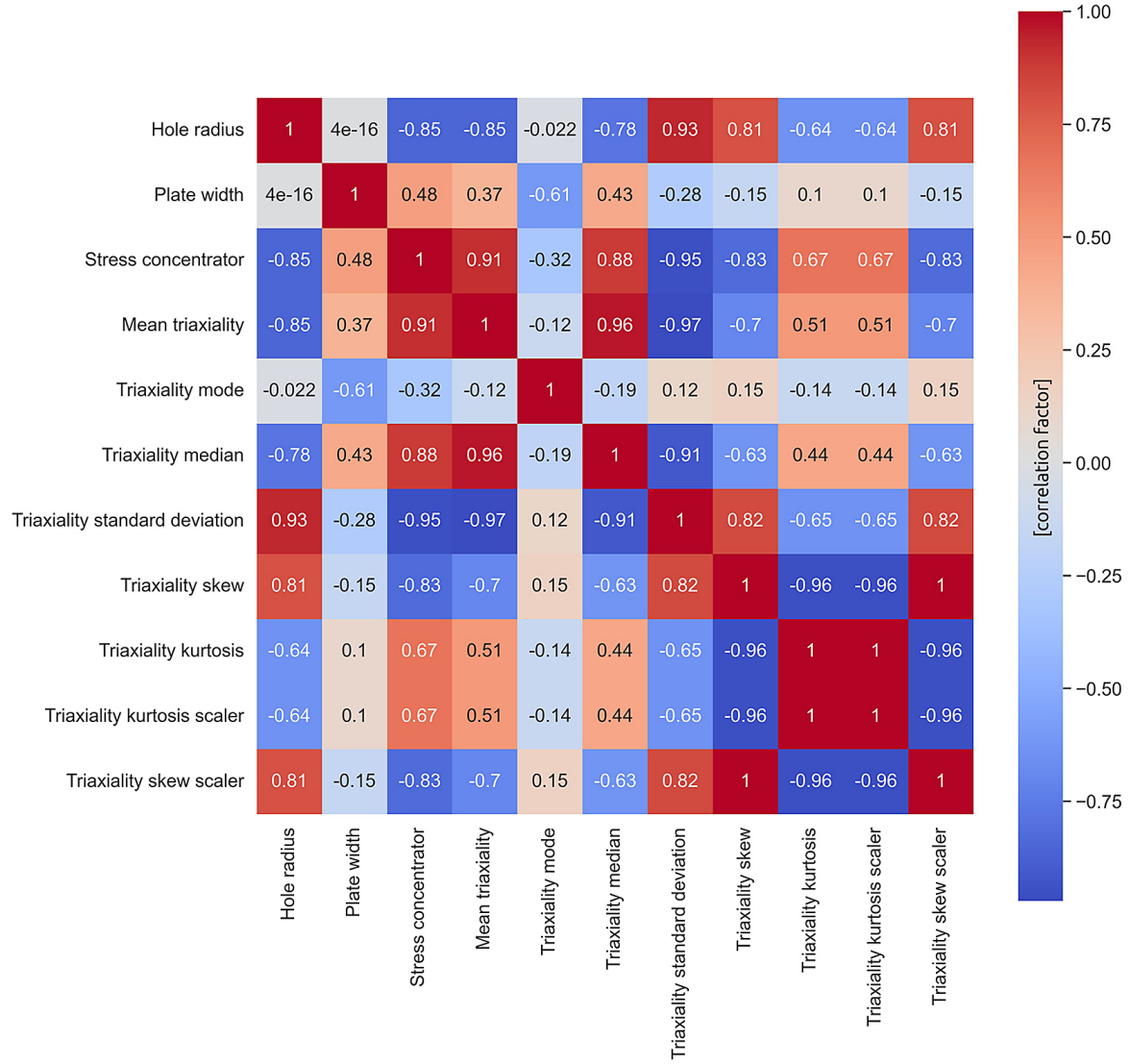

Figure 12. Heatmap of flat specimen with circular hole (in each field, the numerical value of the obtained correlation coefficient and the corresponding color according to the color scale on the right are entered)

Table 6. Stress-state triaxiality measures for all specimens

Sample	Load	Mean	Mode	Median	Std. dev.	Skewness	Kurtosis
Flat specimen with a central hole	Tension	0.91	-0.32	0.86	-0.95	-0.83	0.67

Table 7. Linear regression coefficients

Variable	Hole radius	Width	Mean	Mode	Median	Deviation	Kurtosis	Skewness
Symbol	x_1	x_2	x_3	x_4	x_5	x_6	x_7	x_8
Parameter	a_1	a_2	a_3	a_4	a_5	a_6	a_7	a_8
Value	-9.2e-04	0.002	-5.01	-0.032	3.92	-5.27	-0.052	-0.069

This constitutes a very strong positive relationship, which explains 82.8% of the variability in stress concentration values. This relationship suggests that stress concentrations fundamentally alter the hydrostatic component of the stress state, leading to higher triaxiality values in areas of increased concentration.

Triaxiality mode. The triaxiality mode is characterized by only a weak negative correlation of -0.32, suggesting a lesser influence of the mode on the notch shape factor α value.

Triaxiality median. The triaxiality median shows a very strong positive correlation with the notch shape factor of 0.88, confirming conclusions of mean triaxiality.

Triaxiality standard deviation. The triaxiality standard deviation shows the strongest relationship with the notch shape factor α, reaching a value of -0.95 which explains 90.2% of the coefficient's behavioral variability. Such an exceptionally strong inverse relationship indicates that higher stress concentrations are associated with a more uniform triaxiality distribution in the stress field.

Triaxiality skewness. Triaxiality skewness shows a very strong inverse correlation with the notch shape factor α of -0.83, indicating that lower values are associated with a more left-skewed distribution. Triaxiality kurtosis. Triaxiality kurtosis, in turn, shows a positive correlation of 0.67, meaning that stress concentrations generate more "peaked" distributions for higher notch shape factor α values.

After preliminary analysis using heatmaps, its summary was compiled in Table 6. Strong correlations between stress concentrators and triaxiality parameters have significant implications for failure prediction methods. Contemporary criteria, such as Johnson-Cook fracture model [29] or Rice-Tracey void growth model [30], extensively utilize triaxiality as a key parameter.

The presented results of linear regression analysis indicate high quality of the notch shape factor prediction model. The model uses 8 features characterizing geometry and triaxiality distribution to predict the notch shape factor α values. The coefficient of determination value is R^2 = 0.9784 (97.84%), meaning that the model explains almost the entire variance in the target variable. This is an exceptionally high result, indicating excellent model fit to the data. Only 2.16% of the variance remains unexplained, suggesting that the selected features very well describe the stress concentration phenomenon.

Error metrics:

- MAE = 0.0192: The mean absolute error is very low, meaning that the model's predictions deviate on average from actual values by ±0.0192 units;
- MSE = 0.0011: The very low mean squared error value confirms the model's high accuracy;
- RMSE = 0.0324: The root mean squared error in original units is minimal, indicating precise predictions.

Comprehensive correlation analysis reveals that the notch shape factor exhibits complex relationships with both geometric parameters of structural elements and statistical measures of stress-state triaxiality. Stronger dependencies relate to triaxiality distribution characteristics. The obtained results constitute a foundation for developing more accurate machine learning models to achieve optimal design solutions. As a result of applying the linear regression task, regression model parameters for the notch shape factor α given in the Table 7 were obtained. The intercept (a_0) of the linear regression model is equal to 3.19.

Formula for the notch shape factor α can be written as:

$$\alpha_{reg} = a_0 + a_1 \cdot x_1 + a_2 \cdot x_2 + a_3 \cdot x_3 + \\ + a_4 \cdot x_4 + a_5 \cdot x_5 + a_6 \cdot x_6 + a_7 \cdot x_7 + a_8 \cdot x_8 \quad (12)$$

Many of these parameters can be omitted due to their negligible impact on the model. Therefore, it can be written as:

$$\alpha_{reg} = 3.19 - 5.01 \cdot a_3 + 3.92 \cdot a_5 - 5.27 \cdot a_6 \quad (13)$$

CONCLUSIONS

The model shows very good prediction with R^2 = 97.84%, which indicates very good representation of stress concentration mechanisms. Low values of MAE, MSE, RMSE errors confirm high prediction accuracy. However, such high R^2 may also suggest the need to check whether the model is not over-fitted to the training data. Additional validation on an independent dataset and residual analysis are recommended for complete assessment of model quality.

Multiple linear regression proved to be very stable and accurate in most of the studied configurations, especially where the relationships between features and α were close to linear. Triaxiality statistics dominate the influence on stress concentration; the mean triaxiality parameter remains the strongest predictor across the entire dataset.

The application of linear regression ultimately yielded very low RMSE errors (<0.065), making them practically useful for estimating the notch shape factor α under engineering conditions. However, industrial implementation requires rigorous external validation and residual analysis to avoid overconfidence in the models.

Future work is recommended to extend the dataset with fatigue cases, apply Bayesian methods, and implement more precise feature scaling, especially when triaxiality distribution exhibits strong positive kurtosis.

The conducted research confirms that with appropriate hyper-parameter configuration and proper predictor selection, both analyzed techniques constitute valuable tools for supporting the design of structures sensitive to stress concentrators, with the choice of a specific model depending on the degree of linearity of the phenomenon and validation requirements.

In the analyzed model, the largest regression coefficients were assigned to central value parameters of triaxiality distribution (mean, median), while the influence of geometry (radii, dimensions) was significantly smaller or negligible.

Based on the above relationship, it can be stated that the actual safety factor under fatigue conditions depends on the stress concentration coefficient, since the latter depends on triaxiality field distribution.

REFERENCES

1. Budynas R. G., Nisbett K. J., Shigley's Mechanical Engineering Design, New York: McGraw-Hill Education, 2014.
2. Kocańda S., Szala J., Podstawy obliczeń zmęczeniowych, Warszawa: Państwowe Wydawnictwo Naukowe, 1997.
3. Rolfe S. T., Barsom J. M., Fracture and Fatigue Control in Structures: Applications of Fracture Mechanics, ASTM International, 1977.
4. Schijve J., Fatigue of Structures, Amsterdam: Springer, 2009.
5. Anderson T. L., Fracture Mechanics: Fundamentals and Applications, Boca Raton: CRC Press, 1994.
6. Josephs H., Huston R. L., Blake's Design of Mechanical Joints, Boca Raton: CRC Press, Taylor & Francis Group, 2019.
7. Neimitz A., Janus U., Analysis of stress and strain fields in and around inclusions of various shapes in a cylindrical specimen loaded in tension, Archives of Metallurgy and Materials, 2016a; 61(2): 569–575.
8. Free B., Marino G., Schindelholz E., Dorman S. G. and Locke J. S., Measurement of atmospheric corrosion fatigue crack growth rates on, International Journal of Fatigue, 2023; 167: 107368.
9. Neimitz A., Janus U., Voids nucleation at inclusions of various shapes in front of the crack in plane strain, Archives of Metallurgy and Materials, 2016b; 61(3): 1241–1246.
10. Burns J. T., Boselli J., Effect of plate thickness on the environmental fatigue crack growth behavior of AA7085-T7451, International Journal of Fatigue, 2016, 83: 253–268.
11. Alqahtani I., Starr A. and Khan M., Investigation of the combined influence of temperature and, Materials, 24 October 2023; 16(6833): 1–25.
12. Yang B., Wang S., Li J., Ding X., Xiao Q. and Xiao S., Study on fatigue crack growth in rail steel at numerical and, Materials, 2023; 16: 2981.
13. Pilkey W. D., Pilkey D. F., Peterson's Stress Concentration Factors, Third Edition, Hoboken, New Jersey: John Wiley & Sons, Inc., 2008.
14. Zeng Y., Li M., Wu H., Li N. and Zhou Y., Experiment and theoretical investigation on fatigue life prediction of fracturing pumpheads based on a novel stress-field intensity approach, Materials, 2022; 15(13): 4413.

15. Janus-Galkiewicz U., Galkiewicz J., Analysis of the failure process of elements subjected to monotonic and cyclic loading using the Wierzbicki–Bai Model, Materials, 2021; 14: 6265.
16. Bhandari V. B., Design of Machine Elements, Noida: McGraw Hill, 2010.
17. Parareda S., Frómeta D., Casellas D., Sieurin H. and Mateo A., Understanding the fatigue notch sensitivity of high-strength, Metals, 2023; 13: 1117.
18. Tomaszewski T., Sempruch J., Size effect in high-cycle fatigue, Journal of Machine Construction and Maintenance, 2017; 1: 104.
19. W. Yu, Y. Yin, J. Zhou, Q. Xu, X. Feng, H. Nan, J. Zuo, X. Wang and X. Ding, „Surface Condition Evolution and Fatigue Eval-uation after Different Surface Processes for TiAl47Cr2Nb2 Alloy," Materials, 2022; 15(16): 5491.
20. Ziółkowski A., Parametrization of Cauchy stress tensor treated as autonomous object using isotropy angle and skewness angle, Engineering Transactions, 2022; 70(3): 239–286.
21. Bao Y., Wierzbicki T., A comparative study on various ductile crack formation criteria, Journal of Engineering Materials and Technology, 2004; 126(3): 314–324.
22. Bao Y., Wierzbicki T., On fracture locus in the equivalent strain and stress triaxiality space, International Journal of Me-chanical Sciences, 2004; 46: 81–98.
23. Bai Y., Teng X. and Wierzbicki T., On the application of stress triaxiality formula for plane strain fracture testing, Journal of Engineering Materials and Technology, 2009; 131; 2.
24. Galkiewicz J., Janus-Galkiewicz U. and Lipiec S., The influence of in-plane constraints on fatigue crack growth rate, Advances in Science and Technology Research Journal, 2025; 19(3): 37–46.
25. Iqbal M., Karuppanan S., Perumal V., Ovinis M., Iqbal M., Development of novel surrogate models for stress concentration factors in composite reinforced tubular KT-Joints, Civil Engineering Journal, 01 April 2025; 11(4).
26. Rasul A., Karuppanan S., Perumal V., Ovinis M., Iqbal M., Badshah S., Alam K., Stress concentration factors in tubular T-Joint braces under compressive loads using artificial neural networks, Civil Engineering Journal, 01 June 2025; 11(6).
27. Chu T. S. C., Sorilla J., Chua A. Y., UAV-based structural health monitoring using a two-stage CNN model with lighthouse localization in GNSS-Denied Environments HighTech and Innovation Journal, June 2025; 6(2).
28. Young W. C., Budynas R. G., Roark's Formulas for Stress and Strain, New York: McGraw-Hill Companies, Inc., 2002.
29. Hu F., Liu X., Wang B. and Xiang Y., Investigations on the Johnson-Cook constitutive and damage-fracture model parameters of a Q345C steel, Metals, 2024; 14(5): 509.
30. Rice J., Tracey D., On the ductile enlargement of voids in triaxial stress fields, J. Mech. Phys. Solids, 1969; 17: 201–217.